JGR Solid Earth

RESEARCH ARTICLE
10.1029/2018JB016922

An Effort to Reconcile Time- and Slip-Dependent Friction Evolution

Tianyi Li[1,2]

[1]Department of Geosciences, Princeton University, Princeton, NJ, USA, [2]Now at Sloan School of Management, Massachusetts Institute of Technology, Cambridge, MA, USA

Key Points:
- A new model for RSF is developed, assuming combined physical mechanisms that aimed to reconcile time- and slip-dependent friction evolution
- Finite series of friction data, besides only peaks and minima, are inverted using both our model and the analytical laws, for two stiffnesses
- We show that this model has a slightly better performance in fitting the friction data than the existing laws, with a better physical basis

Supporting Information:
- Supporting Information S1

Correspondence to:
T. Li,
tianyil@mit.edu

Citation:
Li, T. (2019). An effort to reconcile time- and slip-dependent friction evolution. *Journal of Geophysical Research: Solid Earth*, *124*. https://doi.org/10.1029/2018JB016922

Received 22 OCT 2018
Accepted 28 JAN 2019
Accepted article online 1 FEB 2019

Abstract In rate and state friction (RSF) theory, time-dependent evolution (represented by the Aging law) and slip-dependent evolution (represented by the Slip law) both succeed in explaining some features of the friction curves while failing in explaining others. Nevertheless, experimental results provided strong evidence for the two ideas and suggested that they are both critical components in friction evolution. Making a first attempt toward reconciling these two ideas, we developed a new friction model for RSF evolution assuming combined physical mechanisms that highlight asperities' plastic behavior: the time-dependent growth of asperity contact area and the slip-dependent enhancement (slip strengthening) of asperity intrinsic strength. Our model adopts a two-scale mathematical structure developed by Li and Rubin (2017; https://doi.org/10.1002/2017JB013970), where the specification of the surface distribution of asperity ensembles and their geometry facilitates the numerical construction of the state variable in the RSF equation. Results show that this new model's fit to the slide-hold-slide experiments is similar to the best fits of the Slip law, while it provides an improved physical picture; however, for velocity steps it fails to match the symmetry of step ups and downs, although the general fit is acceptable. By introducing two new parameters to specify the slip-hardening mechanism, we allow the model to incorporate as a subset the pure time-dependent model discussed in Li and Rubin (2017). Although failing to completely reconcile time- and slip-dependent friction evolution, this study produced useful insights for future research; for example, a granular numerical description of the frictional surface might be convenient for modeling the physics of friction.

1. Introduction

One critical debate has been running throughout the development of rate and state friction (RSF) theory: Is friction evolution essentially time dependent or slip dependent? A great amount of efforts has been made in exploring both ideas, and two empirical laws were proposed: the Aging law (highlighting time dependence, Dieterich, 1979, the modern form established by Marone, 1998), and the Slip law (highlighting slip dependence, Ruina, 1983, an idea dating back to Rabinowicz, 1951, 1958). Earthquake nucleation simulations suggest that these two laws predict very different nucleation patterns (Ampuero & Rubin, 2008; Rubin & Ampuero, 2005), and thus, the debate for the right RSF evolution law is of high importance. After decades of studies, both laws have gained supporting evidence from experiments while failing to explain certain features of the friction curves, in fitting laboratory data of the two primary categories of friction experiments: the velocity steps and the slide-hold-slide (SHS; Karner & Marone, 2001). The general applicability of each law to various frictional settings has thus been questioned.

For the Slip law, recent results show that it unequivocally produces extraordinary good fits to velocity step experiments, but it is not able to match the SHS data to an acceptable extent (Bhattacharya et al., 2015, 2016). It was also criticized for lacking a clear physical background in the construction of the state variable compared with the Aging law (e.g., Ikari et al., 2016), although various attempts have been made over the years to help the empirical law find proper physical basis (e.g., Aharonov & Scholz, 2018; Hatano, 2015; Sleep, 2005). Our previous study made a similar attempt and showed that this drawback might be overcome through a transparent description of the frictional surface, upon which the Slip law could be essentially established by assuming the state variable as the ensemble of intrinsic strength of individual asperities (Li & Rubin, 2017). However, even if the existing Slip law may not be the correct form for the slip dependence, normal stress step experiments suggested that at least slip dependence plays a role in friction evolution,

since in these experiments it was found that the shear stress change does not evolve at the same rate as the contact area growth (Nagata et al., 2014).

On the other hand, there has been direct evidence for the time dependence of the friction evolution. The log time-dependent growth of the contact area of asperities on the frictional surface was observed and documented more than two decades ago (Dieterich & Kilgore, 1994), which was interpreted ever since as the decisive evidence for the Aging law (Dieterich & Kilgore, 1996; Marone, 1998; Nakatani & Scholz, 2006), in which the state variable is defined as related to the contact area and is therefore proportional to the logarithm of contact time. However, a number of problems have been raised. It has been shown that unlike the Slip law, the Aging law fails to produce symmetry of the frictional response to increasing and decreasing velocity steps, and its prediction of linear slip weakening is contradictory to the exponential slip weakening observed in laboratory experiments for both gouges and bare rock, where the characteristic slip distance is found to be independent of the magnitude of the step, another feature recovered by the Slip law (Bayart et al., 2006; Kato & Tullis, 2001; Marone, 1998; Rathbun & Marone, 2013; Tullis & Weeks, 1986). Recent studies show that its fit to the SHS data is also inferior to that of the Slip law (Bayart et al., 2006; Bhattacharya et al., 2015). Moreover, among the studies of frictional physics, there is evidence suggesting that the time dependence of friction could originate from other physical mechanism besides asperity growth (van den Ende & Niemeijer, 2018) or that asperity growth could be not only time dependent (Renard et al., 2012). Given these lines of results, it is then debated whether the current Aging law is of the right form, where the time dependence, assumed to be associated with the contact area growth, is the single mechanism driving the friction evolution.

Here we try to reconcile the time dependence and the slip dependence of the RSF theory, following a number of previous relevant efforts (e.g., Kato & Tullis, 2001; Nagata et al., 2012). Our idea is to incorporate the time dependence assumption into the model framework developed by Li and Rubin (2017), where the slip dependence is already built into the structure of the model. Based on such idea, in this study, we propose a new model with a transparent structural framework and combined physical mechanisms that aim to rejoin the two components of the friction evolution: we assume that the contact area of asperities grows with the logarithm of contact time, and at the same time, the intrinsic strength of asperities increases with slip (slip strengthening) while the asperities are in contact. In other words, the newly grown contact areas initially have low intrinsic strength; it is after sufficient slip has taken place between the contacting asperities that these areas become much stronger. The second half of our assumption, the slip-strengthening effect, relies on the fact that the full level of intrinsic strength is not reached instantaneously after a normal stress step but requires a certain slip distance, as has been observed in various experiments (Bhattacharya et al., 2017; Nagata et al., 2012). Physically, slip strengthening could be associated with the microscopic process termed as strain hardening or work hardening, a plastic behavior commonly found among metals and other solids (Mott, 1952; Nes, 1997), including nanostructures (Li et al., 2017), although the physical picture of this phenomenon is not fully understood (Du et al., 2011; Mecking & Kocks, 1981; Van Melick et al., 2003). By combining the time-dependent growth of contact area and the slip strengthening of asperity strength, we expect that the fit to SHS data could be improved: potentials of the intrinsic strength are created during the hold (S-H), and they become real intrinsic strength during a fast slip after reslide (H-S), which may then result in the high peak stresses in the data, a level so far too high to be fit by existing laws or models (Bhattacharya et al., 2016).

This model inherits the two-scale memory-recording mathematical structure for friction evolution developed by Li and Rubin (2017), while adopting a new set of physical ideas. In the current model, a numerical framework is used to track the contact area growth and the evolution of intrinsic strength on portions of asperities. The intrinsic shear force f is computed for each individual portion of asperities from different size classes, which constitutes the macroscopic state variable Θ through a weighted summation of asperity classes based on an exponential distribution of the asperity size. The mathematical construction of the macroscopic state Θ from the microscopic intrinsic force f is not pivotal to the content of this paper and thus excluded; details could be found in Li and Rubin (2017).

Simulations and inversions for velocity steps (data from Penn State University) and SHS (Beeler et al., 1994, data) experiments are conducted using this new model. For SHS, two kinds of inversions are tried: only fitting the stress peaks and minima, a convenient approach in fitting SHS data (e.g., Beeler et al., 1994; Bhattacharya et al., 2015), and inverting the entire finite stress series from the start of the hold till

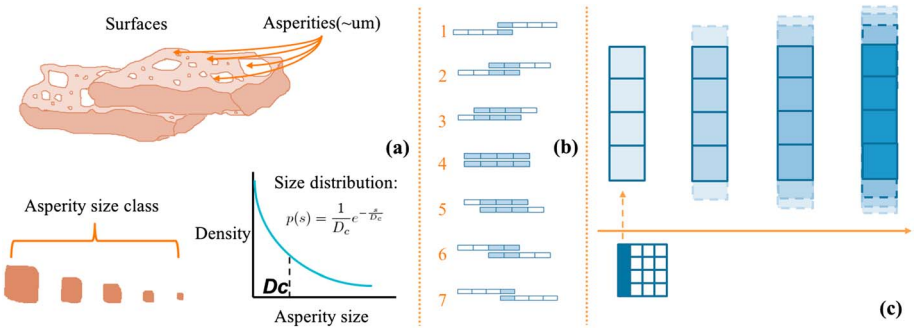

Figure 1. The microscopic picture and major assumptions of the model; panels (a) and (b) are adapted from Figure 1 in Li and Rubin (2017). (a) The two-scale mathematical construction of the friction evolution (assumptions (1)–(3) and (6) in section 2.2). (b) Different contact stages of an exemplary asperity contact pair ($s = 4\Delta\delta$), showing the side image of the 4×4 grid (assumptions (4) in section 2.2). On each of the seven stages, the upper and lower panels of grids correspond to two asperities from both sides of the frictional surface. Filled rectangles denote the in-contact portions of the asperities. (c) The slip-strengthening mechanism shown on the exemplary asperity. One column of the asperity is used for demonstration, and the other columns are omitted. The asperity moves from left to right, during which time the strength of the asperity grids is increasing (slip strengthening) and the contact area of the asperity grid is also increasing (time-dependent growth). Each asperity grows only in the slip-perpendicular direction but not in the slip direction, and thus, it looks like the grown area only appears on the outer elements of the grid. Darker colors denote higher intrinsic strength levels, on both the original contact area (with solid edges) and the new area (with dashed edges). The younger the contact area is, the less slip it experiences and thus the less slip strengthened it is.

the end of reslide, which is a more difficult approach but also has been adopted by many successful efforts (e.g., Marone, 1998; Marone & Saffer, 2015; Niemeijer et al., 2008, 2010). Nevertheless, to the best of our knowledge, no previous studies have shown the result of fitting multiple finite SHS stress series together using the same parameters, and in the current study we made a first attempt.

2. Model

2.1. Frictional Physics on the Sliding Surface

Friction is considered to originate from the shear resistance of the surface ensemble of atomic bonds (asperities). In our model, each asperity is discretized into square portions by a minimum grid spacing and therefore represented by a set of grid elements (Figure 1). The shear force f of a specific portion of an asperity (e.g., a single grid element) is given by

$$f = A \cdot \tau \tag{1}$$

where A and τ are the contact area and the microscopic stress of the grid element. Both properties are not fixed and evolve in the frictional process. In our model, we make one assumption for each of these two terms:

(I) For stationary or sliding surfaces, contact area grows with time; new contact area ΔA is constantly added to the initial area A_0:

$$A = A_0 + \Delta A. \tag{2}$$

The contact area A is assumed to grow at a rate proportional to the logarithm of contact time (Baumberger & Caroli, 2006), and the numerical construction of the newly grown area ΔA is discussed in section 2.3. Contact time starts when the first grid enters the contact pair and ends when the last grid leaves the contact. The time spent in contact on each grid is given by the grid size divided by the slip velocity, and thus, the entire time of the asperity spent in a contact is the asperity size divided by the slip velocity.

(II) The stress τ on a grid element evolves under two effects: the direct effect, which depends on the logarithm of the current slip velocity V, and a slip-strengthening effect, which depends on the distance δ the element has slipped since becoming part of the contact

$$\tau(V, \delta) = \hat{\tau}(\delta) \left[1 + \hat{a} \ln \left(\frac{V}{V_0} \right) \right]. \tag{3}$$

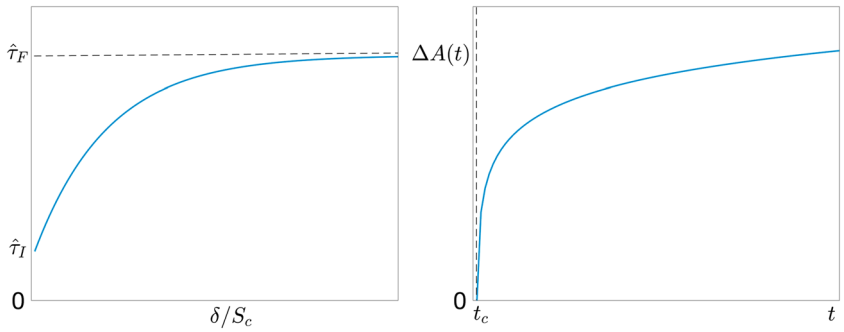

Figure 2. (left) The slip-strengthening curve of the asperities' intrinsic strength (equation (10)). The initial and fully evolved intrinsic strength are $\hat{\tau}_I$ and $\hat{\tau}_F$, respectively. (right) The log time dependence of contact area growth; new contact area ΔA as a function of contact time t (equation (8)). Cutoff time is t_c.

Here $\hat{\tau}(\delta)$ is the "intrinsic strength" of the grid element, defined as its shear resistance at the reference sliding speed V_0, and â is the microscopic coefficient of the direct effect. The direct effect on τ is standard in the rate and state literature (Ruina, 1983); the slip-strengthening effect is the new assumption of the current model (see section 2.3). Note that on a grid element, each portion of the new contact area, added at a different timestep, is associated with a certain slip distance δ; thus, the intrinsic strength $\hat{\tau}(\delta)$ of the entire new contact area of a grid element is heterogeneous with respect to different portions (see (10) and (11) below).

Putting (2) and (3) back into (1), we have

$$\begin{aligned} f &= (A_0 + \Delta A)\hat{\tau}\left[1 + \hat{a}\ln\left(\frac{V}{V_0}\right)\right] \\ &= A_0 \cdot \hat{\tau}_{A_0}\left[1 + \hat{a}\ln\left(\frac{V}{V_0}\right)\right] + \Delta A \cdot \langle\hat{\tau}_{\Delta A}\rangle\left[1 + \hat{a}\ln\left(\frac{V}{V_0}\right)\right] \\ &= A_0 \cdot \hat{\tau}_{A_0} + A_0 \cdot \hat{\tau}_{A_0} \cdot \hat{a}\ln\left(\frac{V}{V_0}\right) + \Delta A \cdot \langle\hat{\tau}_{\Delta A}\rangle. \end{aligned} \tag{4}$$

The reason we have $A_0 \cdot \hat{\tau}_{A_0}$ in two terms instead of incorporating it into one is to let the expression of (4) match the three terms in the expression of the macroscopic friction coefficient μ (equation (6); see below). As mentioned above, in the second line of (4) we distinguish between the two intrinsic strength $\hat{\tau}$ on different areas of the grid elements: the intrinsic strength of the initial contact area of a grid element, $\hat{\tau}_{A_0}$, and the (area-weighted) average intrinsic strength of the newly added area, $\langle\hat{\tau}_{\Delta A}\rangle$, the latter being an ensemble, and we have $\hat{\tau}_{A_0} = \hat{\tau}(\delta) > \langle\hat{\tau}_{\Delta A}\rangle$ (see equation (11)). Also note that we omit the second-order term $\Delta A \cdot \hat{a}\ln(V/V_0)\hat{\tau}$ in comparison to the second and third terms in the last line of (4) since typically $\Delta A/A_0 \ll 1$ and $\hat{a}\ln(V/V_0) \ll 1$ (e.g., Baumberger & Caroli, 2006).

Summing up the microscopic shear force f over all grid elements of all asperities, the total shear force on the surface is obtained, which becomes the macroscopic shear stress σ_s after dividing by the apparent surface area A_a. The macroscopic friction coefficient μ is thus given by

$$\mu = \frac{\sigma_s}{\sigma_n} = \frac{\sum f}{A_a\sigma_n}, \tag{5}$$

where σ_n is the (macroscopic) normal stress. The details of the summation operator $\sum$ (over all grid elements of all asperities) are omitted due to the limited space.

The friction coefficient μ in RSF can be expressed as (Nakatani, 2001; Nakatani & Scholz, 2006; Rice et al., 2001):

$$\mu = \mu_* + a\ln\frac{V}{V_*} + (\Theta - \Theta_*), \tag{6}$$

where V and Θ are the slip velocity and the macroscopic state variable in RSF; stars indicate reference values, and a controls the magnitude of the direct velocity effect. Note that (6) is not the most common form of the RSF equation; in particular, the parameter b controlling the macroscopic evolution effect does not appear in this expression, as in more well-known forms of RSF equations (Dieterich, 1979; Ruina, 1983; Marone,

1998). We use this form because the state variable Θ in our model is defined more conveniently under this form of the RSF equation. Comparing (4) and (6), the three terms constituting the microscopic f in (4) can be readily mapped to the three terms of μ: the reference constant, the direct effect, and the evolution effect. Note that in (4), $A_0 \cdot \hat{\tau}_{A_0}$ on one particular grid element is not constant but slip dependent since $\hat{\tau} = \hat{\tau}(\delta)$. However, the after-birth slip distance δ of a certain grid element is completely determined by the size s of the asperity which the grid belongs to (see filled areas of Figure 1b for conceptualization): $\delta = \delta(s)$; a large in-contact slip distance δ only appears on the grid elements of large asperities. Therefore, since $\hat{\tau}$ only depends on δ, for an invariant distribution $p(s)$ of the asperity size s, the distribution of $\hat{\tau}$ (then $\hat{\tau}_{A_0}$) is also invariant in time. The $A_0 \cdot \hat{\tau}_{A_0}$ term can thus transfer into a constant $\mu_* = \int A_0 \cdot \hat{\tau}_{A_0} p(s)\mathrm{d}s = A_0 \int \hat{\tau}(\delta) p(s)\mathrm{d}s = A_0 \int \hat{\tau}(s) p(s)\mathrm{d}s$ (constant if $p(s)$ invariant). By the same token, the second term in (4) corresponds to the direct effect; comparing (4) and (6), we see that the macroscopic and microscopic direct effect coefficients are related via $a = \mu_* \hat{a}$.

To solve for V and Θ, we apply the following friction evolution equations:

$$a\frac{\mathrm{d}V}{\mathrm{d}\delta} + V\frac{\mathrm{d}\Theta}{\mathrm{d}\delta} = k(V_{lp} - V), \tag{7a}$$

$$\Theta = F(V(\delta)). \tag{7b}$$

Equation (7a) is the spring-block slider system with finite stiffness k and load point velocity V_{lp}, obtained by taking the derivative of (6) as well as equation (25) in Ruina (1983) and equating the two derivatives (note the derivative is taken with respective to slip δ, not t). In (7b), $F(V)$ is a numerical kernel tracking the evolution of the state variable in (6), as a function of slip δ. We describe the formulation of this kernel in section 2.2. Equation (7b) takes place of the traditional differential equation $\dot{\theta} = f(V, \theta)$ in standard RSF evolution equations (Dieterich, 1979; Ruina, 1983). In our model, $\dot{\Theta}$ cannot be expressed as a function of Θ and V because different distributions of f at the subasperity scale can give rise to the same Θ but different evolutionary paths for Θ; therefore, $\dot{\Theta}$ is finite-history dependent and is not analytically trackable.

2.2. The Two-Scale Picture of Friction Evolution

To construct the macroscopic state variable Θ (the third term in (6)) from the partial microscopic intrinsic force $\Delta A \cdot \hat{\tau}(\delta)$ (the third term in (4)), we apply the two-scale mathematical description of the frictional (bare rock) surface developed by Li and Rubin (2017). This structure specifies the geometry of individual asperities as well as the size distribution of the ensemble of asperities on the surface. The kernel F in (7b) is numerically constructed to realize the mathematical description, and we use it in this study to compute Θ from $\Delta A \cdot \hat{\tau}(\delta)$.

The basic assumptions of the two-scale description of the friction evolution are summarized as follows: (1) the frictional surface consists of an ensemble of asperities, following a specific size distribution (in this study, an exponential distribution with characteristic length D_c); (2) asperities are assumed to be square such that they are further discretized into portions by the minimum grid spacing $\Delta\delta$, each portion having the square area $A_0 = (\Delta\delta)^2$; (3) keeping first-order consistency, it is assumed that only asperities of the same size on opposing sides of the sliding surface form a contact, adopting the Greenwood and Williamson picture of asperity bumps between random surfaces (Greenwood & Williamson, 1966) and that asperities are aligned in the slip-perpendicular direction; (4) for a specific asperity size class, two asperities forming a contact pass through a number of stages where the contact area first grows and then shrinks, in increments of $\Delta\delta$, and at any moment on the surface, all these stages are of equal abundance; (5) the new contact area ΔA emerges on each grid element on top of the initial (real) contact area A_0 and starts to grow when this grid element enters the contact and the contact time begins to accumulate; (6) the intrinsic force on all grid elements is summed up to obtain the intrinsic force for that entire asperity, with all contact stages equally weighted. The total intrinsic (i.e., at the reference slip speed) shear force of the surface is then constructed by taking into account all asperity size classes, following the exponential size distribution, and is finally divided by $A_a\sigma_n$ (equation (5)) to determine the surface state variable Θ. The specific description of the two-scale mathematical structure is not central to the content of this study and thus excluded, which can be found in Li and Rubin (2017), where these assumptions except for (5) are discussed with more detail. Regarding (5), for concreteness, one could imagine that each asperity grows only in the slip-perpendicular direction but not in the slip direction, and thus, it looks like the grown area only appears on the outer elements of the grid, as illustrated in Figure 1c. This should be viewed only as a convenient numerical approximation

to the more realistic possibility that the contact grows in all directions. To address the latter possibility, one could imagine a different microscopic picture, where we distinguish the real contact area from the nominal area of grid elements: in this case the real contact area of each grid element A_0 is less than the nominal area $(\Delta\delta)^2$, as opposed to the current assumption that $A_0 = (\Delta\delta)^2$. This is essentially assuming that asperity portions (grid elements) are unfilled but each having a core. However, this picture is also flawed since grid elements should not be unfilled at all discretization scales. Generally speaking, the geometry of the model's microscopic picture is unsettled and we consider it as a major drawback of the model (see section 4).

2.3. Contact Growth and the Slip-Strengthening Curve

In this subsection we specify the growth of new contact area ΔA in Assumption (I) of section 2.1 and the slip-strengthening curve of the asperity intrinsic strength $\hat{\tau}(\delta)$ in Assumption (II) (Figure 2). As is well known since the observations of Dieterich and Kilgore (1994), the new contact area ΔA of an asperity portion grows roughly as the logarithm of contact time t (Baumberger & Caroli, 2006)

$$\Delta A(t) = A_0 \cdot \hat{b} \ln\left(1 + \frac{t}{t_c}\right) \quad , \tag{8}$$

where A_0 is the original contact area $(\Delta\delta)^2$ and $\hat{b} \ll 1$ is the microscopic coefficient of area growth. The t_c is the "cutoff" time; for $t \ll t_c$, $\Delta A/A_0 \ll \hat{b}$. For a grid element that has been part of a contact for m slip increments of size $\Delta\delta$, the contact time t is

$$t = \sum_{i=1}^{m} \Delta t_i = \sum_{i=1}^{m} \frac{\Delta\delta}{V_i} \quad , \tag{9}$$

where the V_i are the sliding velocities over those previous m increments. The minimum contact time $t_{\min}$ in a simulation is $\Delta\delta/V_{\max}$, where $V_{\max}$ is the largest slip velocity in the simulation. We assume t_c to be small enough such that $t_{\min} \gg t_c$, and this lets us use the simpler expression $\Delta A(t) = \hat{b} \ln(t) \cdot A_0$ in place of (8) (the $A_0 \hat{b} \ln(t_c)$ term could be viewed as being folded into the constant in (4)). Note that in some cases the cutoff time found in laboratory experiments could be large (Ikari et al., 2016), and thus, our model is going to lose some accuracy in such settings. For numerical purposes we partition the new contact area ΔA between slip increments: we denote the new contact area that emerges during the ith slip increment as $\Delta A_i - \Delta A_{i-1}$.

Unlike the time dependence of the area growth, there is little experimental data to constrain the slip dependence of contact quality (i.e., indicated by the asperity strength; e.g., Nagata et al., 2014). For simplicity, we assume that the evolution of the asperity intrinsic strength follows an exponential curve, which is not contradictory to the normal stress step experiments of Nagata et al. (2012). The slip-strengthening curve is assumed to be

$$\hat{\tau}(\delta) = \hat{\tau}_I + (\hat{\tau}_F - \hat{\tau}_I)(1 - e^{-\frac{\delta}{S_c}}), \tag{10}$$

where $\hat{\tau}_I$ and $\hat{\tau}_F$ are the initial and fully evolved intrinsic strength of an asperity portion, respectively. This slip-strengthening curve applies to the intrinsic strength of both the original area ($\delta = 0$ when that grid element becomes part of the contact) and the new area ($\delta = 0$ at the time step when that particular increment of ΔA is added to the contact). This difference in slip between A_0 and ΔA associated with each grid element is what gives rise to the distinction between $\hat{\tau}_{A0}$ and $\langle \hat{\tau}_{\Delta A} \rangle$ in (4). Note that we also investigated an alternative slip-strengthening process, in which the δ for both A_0 and ΔA of each element began to accumulate at the time when that element became part of the contact. Although this alternative resulted in qualitatively similar behaviors of the friction evolution, quantitatively it did not match the velocity steps and SHS data as well, so we did not pursue this further.

Looking at equation (10), we define the ratio of the two reference intrinsic strengths to be $r_c = \hat{\tau}_I/\hat{\tau}_F \in [0, 1]$. S_c is the characteristic slip scale of the strengthening curve, and we normalize it by the characteristic length D_c of the asperity size distribution and define $s_c = S_c/D_c > 0$. The r_c and s_c are the two dimensionless parameters introduced in the model to describe the slip-strengthening mechanism. Finally, drawing the assumptions for both time dependence (equation (8)) and slip dependence (equation (10)) of friction evolution, for a grid element that has slipped by $k\Delta\delta$ since joining a contact, the third term in (4) is thus given by

$$\Delta A \cdot \langle \hat{\tau}_{A_0} \rangle = \Delta A_1 \hat{\tau}(\delta_1) + (\Delta A_2 - \Delta A_1)\hat{\tau}(\delta_2) + \ \ldots \ = \sum_{i=1}^{k} (\Delta A_i - \Delta A_{i-1})\hat{\tau}(\delta_i) \quad , \tag{11}$$

where δ_i, the distance slipped by the ith increment of area increase ΔA_i, is equal to $(k - i + 1)\Delta\delta$, and there is $\Delta A_0 \equiv 0$.

2.4. Velocity Neutrality Condition

At two steady states with different slip velocities V_I and V_{II}, the difference in shear force f on a specific asperity portion with slip index k is (recall (4), (8), and (11); note $\hat{\tau}(\delta)$ is independent of V)

$$\begin{aligned}(f_{II}-f_I)_k &= A_0\hat{\tau}_k\hat{a}\ln\frac{V_{II}}{V_I}+\Delta A_{II}\langle\hat{\tau}_{\Delta A,II}\rangle-\Delta A_I\langle\hat{\tau}_{\Delta A,I}\rangle\\ &= A_0\hat{\tau}_k\hat{a}\ln\frac{V_{II}}{V_I}+\sum_{i=1}^{k}(\Delta A_{i,II}-\Delta A_{i-1,II})\hat{\tau}_i-\sum_{i=1}^{k}(\Delta A_{i,I}-\Delta A_{i-1,I})\hat{\tau}_i\\ &= A_0\hat{\tau}_k\hat{a}\ln\frac{V_{II}}{V_I}+A_0[\sum_{i=2}^{k}\hat{b}\ln(\frac{i}{i-1})\hat{\tau}_i+\hat{b}\ln(\frac{\Delta\delta}{V_{II}})\hat{\tau}_{k-1}]-A_0[\sum_{i=2}^{k}\hat{b}\ln(\frac{i}{i-1})\hat{\tau}_i+\hat{b}\ln(\frac{\Delta\delta}{V_I})\hat{\tau}_{k-1}]\\ &= A_0\hat{\tau}_k\hat{a}\ln\frac{V_{II}}{V_I}+A_0\hat{\tau}_{k-1}\hat{b}\ln\frac{V_I}{V_{II}}.\end{aligned} \tag{12}$$

To derive the third line in (12) from the second line, we use the relation, valid at constant V,

$$\Delta A_i-\Delta A_{i-1}=\hat{b}\ln(\frac{i\Delta\delta}{V})-\hat{b}\ln\frac{(i-1)\Delta\delta}{V}=\hat{b}\ln(\frac{i}{i-1})\qquad\text{for}\qquad i>1. \tag{13}$$

Also, note that

$$\hat{\tau}_k=\hat{\tau}(k\Delta\delta)=\hat{\tau}_I+(\hat{\tau}_F-\hat{\tau}_I)(1-e^{-\frac{k\Delta\delta}{S_c}}). \tag{14}$$

To guarantee a high resolution of the slip-strengthening mechanism, a small grid spacing $\Delta\delta$ is required. Therefore, $\hat{\tau}_{k-1}\sim\hat{\tau}_k$. As a result, (12) becomes

$$(f_{II}-f_I)_k\sim\hat{\tau}_kA_0(\hat{a}-\hat{b})\ln\frac{V_{II}}{V_I} \tag{15}$$

and $f_{II}-f_I=0\leftrightarrow\hat{a}=\hat{b}$. Thus, the velocity neutrality of the entire frictional surface is denoted by $\hat{a}=\hat{b}$, as long as the numerical grid is fine enough. Similar to a and $\hat{a}$, the microscopic and macroscopic coefficients governing state evolution are related via $b=\mu^*\hat{b}$.

Setting $s_c=0, s_c=\infty$, or $r_c=1$, (10) becomes $\hat{\tau}(\delta)=\hat{\tau}$. This is a trivial case where any new contact area obtains its final intrinsic strength instantaneously. This exactly recovers the pure aging law discussed by Lin and Rubin (2017, their Case A), where the state variable evolves only with time and no slip strengthening occurs, a case highly similar to the classical Aging law. Under this trivial case, (4) becomes (recall (8))

$$\begin{aligned}f &= A_0\cdot\hat{\tau}+A_0\cdot\hat{\tau}\cdot\hat{a}\ln\frac{V}{V_0}+\langle\Delta A\cdot\hat{\tau}\rangle\\ &= \hat{\tau}[A_0+A_0\cdot\hat{a}\ln\frac{V}{V_0}+\Delta A]\\ &= \hat{\tau}A_0[1+\hat{a}\ln\frac{V}{V_0}+\hat{b}\ln t],\end{aligned} \tag{16}$$

and it is obvious that (15) and the velocity neutral condition are exact. With different choices of s_c and r_c, the current study could be viewed as amplifying the model space of Case A in Li and Rubin (2017).

3. Results

The model is used to conduct three categories of experiments: simulations of the infinite stiffness velocity steps, inversions of the finite stiffness velocity step data, and inversions of the SHS data. The velocity step data are for synthetic gouge from the Rock and Sediment Mechanics Laboratory, Penn State University (Bhattacharya et al., 2015); the SHS data are for initially bare granite from Brown University (Beeler et al., 1994). Although the two data sets are from different experimental settings, it is expected that the RSF theory is universal and thus applies in both settings (see section 4 for discussion). Numerically, our model solves equations (7a) and (7b) and proceeds in slip distance δ rather than time t, producing the output $V=V(\delta)$, $\Theta=\Theta(\delta)$, $\mu=\mu(\delta)$, and $t=t(\delta)$. An input series of $V_{lp}(\delta)$ is required, which we obtain from the data series $V_{lp}(t)$. The machine stiffness k is a priori information in these experiments. Inverted parameters are D_c, $\hat{a}$, $\hat{b}$, s_c, and r_c.

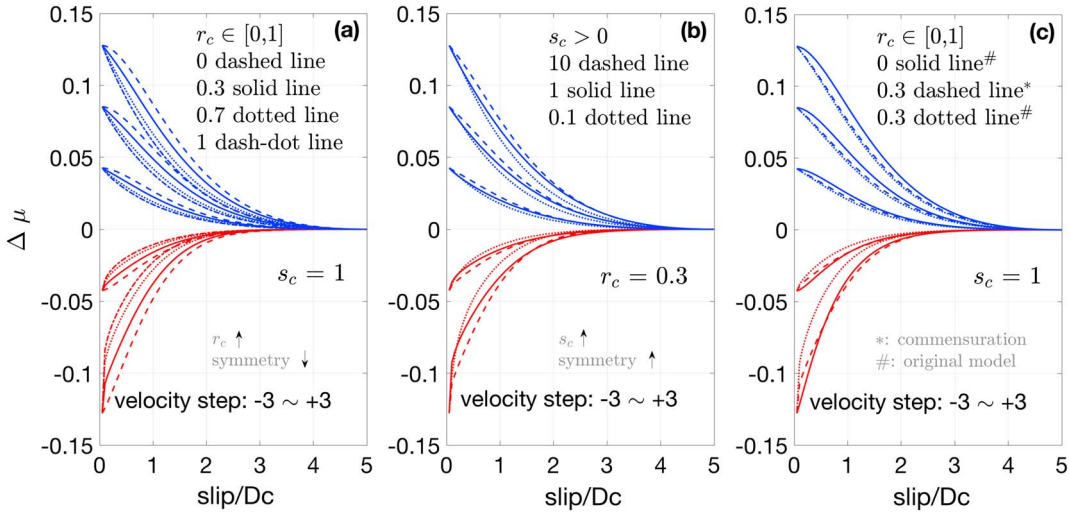

Figure 3. Simulation results of infinite stiffness velocity steps. All subfigures show velocity step curves of magnitude ± 1, $+2$, ± 3 (for a clear sight of the figures, -2 is not shown). (a) Varying $r_c \in \{0, 0.3, 0.7, 1\}$ and keeping $s_c = 1$. (b) Varying $s_c \in \{0.1, 1, 10\}$ and keeping $r_c = 0.3$. Monotonously decreasing r_c or increasing s_c will enhance the symmetry of the curves for velocity step ups and downs. (c) The additional commensuration assumption ($*$ in the figure; see section 4) helps improve the symmetry of velocity steps. Adopting this extra assumption, we are able to obtain the symmetry level comparable to $r_c = 0$ in the original model (# in the figure) when the maximum symmetry is reached, with $r_c = 0.3$. Thus, this variant of the model has an improved symmetry for velocity steps.

Numerically, $\Delta\delta$ is the minimum slip increment, which is also the uniform grid size of asperity portions; $D_{\max}/D_{\min}$ are the maximum/minimum asperity size. A fine grid spacing $D_c/\Delta\delta \gtrsim 20$ and a relatively large asperity size range $D_{\max}/D_c \gtrsim 6$ are required to make sure that the numerical results are converged and smooth. However, we are unable to implement a grid spacing finer than $D_c/\Delta\delta \sim 30$ due to the large computational burden it will incur. We set $D_{\min} = \Delta\delta$, such that $D_{\max}/D_{\min} \gtrsim 120$. Given the computational expense of the forward model, the downhill simplex method (Press et al., 1986) is applied to carry out the inversions; different starting points were tried out in multiple inversion runs and ended up with essentially the same optimal results.

3.1. Simulation: Infinite Stiffness Velocity Steps

In the model, two new parameters ($s_c = S_c/D_c$, the characteristic slip length of slip strengthening normalized by the characteristic length of the asperity size and $r_c = \hat{\tau}_I/\hat{\tau}_F$, the ratio between the initial and fully evolved intrinsic strength of asperities) are introduced to describe the slip-strengthening mechanism, and their behaviors are investigated through infinite stiffness velocity steps simulations (Figure 3). Results show one shortcoming of this model that it does not generate symmetric friction curves for velocity step ups and downs, which is an important feature of the Slip law (Ruina, 1983), although whether or not the velocity step curves should demonstrate complete symmetry is still in debate (Rathbun & Marone, 2013). In our model, the asymmetry of the velocity step curves increases with the step size: velocity steps of 1 order of magnitude are quite symmetrical by eye, while ± 3 order velocity steps are highly asymmetric. Nevertheless, while incapable of demonstrating the complete symmetry of the curves, this model opens a new parameter space spanned by s_c and r_c which allows for the tuning of the extent of symmetry, which suggests that the symmetry of the velocity step curves could be related to the slip-strengthening properties of the frictional surface. Monotonously decreasing r_c, that is, having a weaker new area, or increasing s_c, that is, having a larger characteristic length of the slip-strengthening evolution, both of which lie in the direction of enlarging the distance between the initial and fully evolved intrinsic strength, will enhance the symmetry of the curves (Figures 3a and 3b).

3.2. Inversion: Finite Stiffness Velocity Steps

The symmetry of velocity step curves has been emphasized by many previous studies. However, it should note that most experiments so far well fit by the Slip law are carried out for velocity steps of only ± 1 or ± 2 orders of magnitude (Bhattacharya et al., 2015). Given the absence of sufficient lab data for much larger

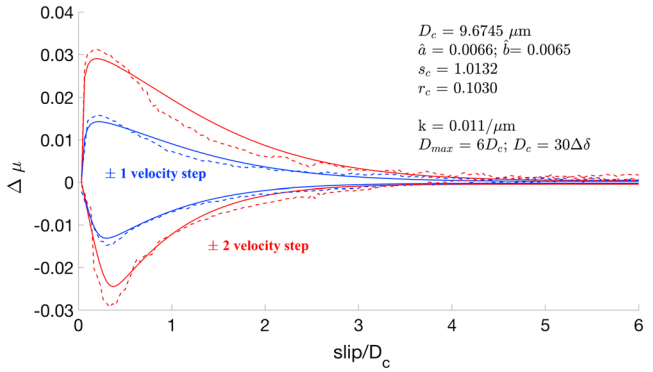

Figure 4. Inversion results of finite stiffness velocity steps (data P1060 from Penn State University). Dashed lines are data, and solid lines are inversion results. The ± 1 velocity steps are well fit, while ± 2 velocity steps are fit slightly worse. Best fit parameters lie in the reasonable parameter space. A near-velocity neutral condition ($\hat{a} \sim \hat{b}$) is obtained, consistent with the physical property of the experimental surface. As expected, this model does not fit velocity step curves as well as the Slip law due to its inability to symmetrically match step ups and downs, although in general these fits arguably look acceptable.

velocity steps, it is then useful to raise the possibility that maybe the complete symmetry for step ups and downs is not a required feature for RSF models in the first place, particularly in fitting finite stiffness velocity steps from the real experimental data. Under this consideration, we used our model to invert data P1060 from Penn State University, which has the best quality among a number of different data pieces and has been shown to be well fit by the Slip law (Bhattacharya et al., 2015). The whole time series of the data was windowed, and only sections around velocity steps were used in the inversion. The entire parameter set â, $\hat{b}$, D_c, s_c, and r_c is inverted. Numerical parameters are set as $D_c = 30\Delta\delta$ and $D_{\max} = 6D_c$. Results show that despite the model's asymmetrical behavior, it fits the ±1 order velocity steps quite well, while the fit to the ±2 order steps is less satisfactory (Figure 4). Simulation results suggest that decreasing r_c enhances the symmetry of step ups and downs, and thus, a small r_c is expected; this is confirmed here since the best fit of r_c is small (~ 0.1). The inverted s_c is around 1, which is a reasonable reference value for s_c. Inverted â and $\hat{b}$ suggest an approximate velocity neutrality on the surface ($\hat{a} \sim \hat{b}$), consistent with the physical condition of the experimental setting that is determined in steady state friction. Nonetheless, we admit that the fit to the data is clearly worse than the best Slip law fit (Bhattacharya et al., 2015), despite having two more fitting parameters. In fact, it seems that the P1060 data are fit so well by the Slip law that it is difficult to identify a competitive candidate law or model without degrading the fit to this piece of data.

3.3. Inversion: SHS

3.3.1. *Fitting Stress Peaks and Minima*

As mentioned, a primary motivation for building the model was the expectation that it might fit SHS data well, a goal not achieved by using either the Aging or the Slip law. We used the Beeler et al. (1994) data for SHS inversions since they applied two different machine stiffnesses in the same experimental setting. First, we only invert the stress minima at the end of each hold and stress peaks after each reslide. The high- and low-stiffness data are inverted at the same time. In order to reduce the numerical error and without much loss of accuracy (as suggested by tests), inversions are carried out for idealized velocity histories where V_{lp} is strictly set as either 0 (during hold) or V_0 (during reslide), rather than being a real (imperfect) load point history. The steady sliding velocity V_0 is $\sim$ 1 μm/s for the lower stiffness setup and ~ 0.316 μm/s for the higher stiffness setup. Numerical parameters are set as $D_c = 30\Delta\delta$ and $D_{\max} = 6D_c$. The entire parameter set r_c, s_c, D_c, â, and $\hat{b}$ is inverted. Results show that, to our disappointment, this model does not produce a fit to the SHS data much better than the Slip law (Bhattacharya et al., 2017, Figure 10b), when only inverting stress peaks and minima; it fits the stress minima reasonably well but fails to match the stress peaks, for both high and low stiffnesses (Figure 5). The best fit parameters of the results all lie in the reasonable parameter space: $D_c \sim 3$ μm, $\hat{a} \sim 0.02$ $(a \sim 0.01)$, $\hat{b} \sim 0.02$ $(b \sim 0.01)$, $s_c \sim 1$, and $r_c \sim 0.1$. Notably, the $a - b$ difference in our best fit results (~ -0.0008) falls near the expected value (~ -0.0027), whereas the $a - b$ value of the Slip law fit (Bhattacharya et al., 2017, Figure 10b) has the wrong sign ($a - b = 0.003$). Since the sign of $a - b$ reflects the physical condition of the sliding surface (velocity strengthening or weakening), we argue that this suggests a potential improvement upon the Slip law fits.

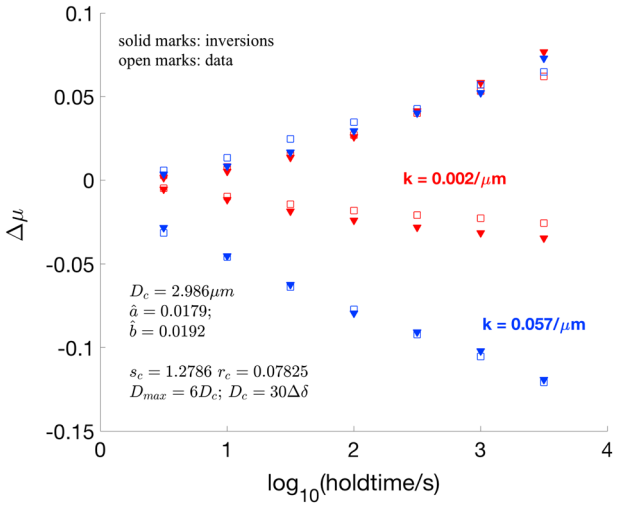

Figure 5. Inversion results of slide-hold-slide (SHS) experiments (data from Beeler et al., 1994). The inversion is carried out only for stress peaks and minima, of two stiffnesses ($k = 0.002/\mu$m and $k = 0.057/\mu$m). Open marks are data, and solid marks are inversions. Best fit parameters fall in the reasonable parameter space and are consistent with prior findings. Within the experimental variability of the SHS tests, we consider the results as a good fit for the current data set. The Slip law has a similar fitting performance for the SHS data, but its physical picture is less transparent than our model.

3.3.2. *Fitting Finite Stress Series*

Next, we inverted the same SHS data but this time fit a finite series, rather than just fitting the stress peaks and minima. For holds the difference is unimportant, because since the load point and the stiffness of the system

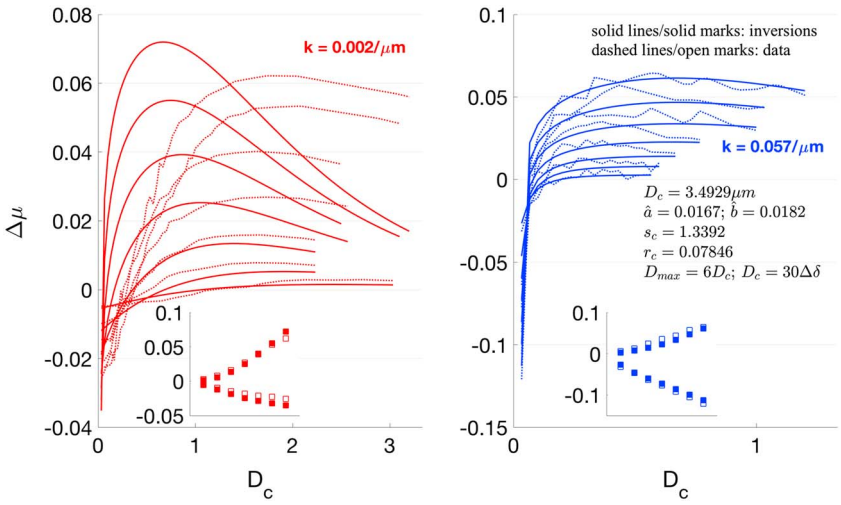

Figure 6. Finite series inversion results of Beeler et al. (1994) slide-hold-slide data using the new model. The inversion scheme is the same as in Figure 5, but this time the entire stress series are fit. Peaks and minima of the finite series are shown in sets. Solid lines and open marks are inversions; dashed lines and solid marks are data. Our model failed to simultaneously match both low- and high-stiffness finite series to a considerable extent: for high stiffness and short hold times of low stiffness, the fits are good, but for low stiffness with longer hold times, the fits deviate much from the data.

are both fixed, there is a one-to-one correspondence between the stress and the slip distance at the end of (and of course, during) each hold. The same is not true for the reslides; however, since the load point moves while the surface is sliding, it is then possible that the peak stress was exactly fit but the proper slip distance was not matched, in which case the misfit is zero but the fit is essentially incorrect. Fitting only the stress peaks during the reslides thus amounts to an unjustified discarding of pertinent data. Upon these concerns, we therefore inverted a finite displacement series starting from the end of each hold (because of the one-to-one correspondence mentioned above, fitting the full hold is redundant) and continuing past the peak stress, stopping at around 80% of the peak stress level. Furthermore, in order to (1) give the stress minima and peaks equal weights in the inversion and (2) also give the SHS series of different hold times equal weights, we (1) multiply the weight of the first point (the stress minimum) for each hold by the number of points in the reslide series for that hold and (2) weight the misfit for each hold by the inverse of their series length. We use the same numerical scheme as previously ($D_c = 30\Delta\delta$; $D_{\max} = 6D_c$; full parameter set inversion), and the best fit results are shown in Figure 6. Similar to only fitting the peaks and minima, in this finite series inversion, our model is once more unable to simultaneously match the data for both the low- and high-stiffness cases. The fit for high-stiffness series is reasonably good, but the low-stiffness series are not well matched. At low stiffness, the friction evolution occurred for a longer time since both the fixing and the reloading is slower; therefore, there might be enough time for some secondary mechanisms to take place whose effects are not significant at high stiffness, which we currently are not able to capture. The peaks and minima in this finite series inversion are shown in insets; these show only a slightly worse fit than in Figure 5.

We conducted the same finite series inversion for the Aging law and Slip law; the best fits are shown in Figure 7. We also computed forward runs for those laws using the best fit parameters in Figure 10 of Bhattacharya et al. (2017), which were obtained by only fitting stress peaks and minima; the results are shown in Figures S1–S4 in the supporting information. Comparing Figures 6 and 7, it shows that our model has a better fit to the general shape of the finite SHS series than either the Aging law or the Slip law, and the match to the stress peaks and minima in the finite series is clearly better than the two analytical laws. Notably, although the Aging law fits in Figure 7 seem to match the low-stiffness data well, a more careful examination will show that those several short hold time forward series of the Aging law (solid red lines) have not reached the stress peaks at the end of the inverted series, whereas the data have passed the peaks. As for the Slip law fit in Figure 7, the fit to the high-stiffness data is obviously unacceptable. Moreover, unlike our model, both the Aging law and the Slip law have $a - b > 0$ in their best fit results, which is not consistent with the physical condition of the experiments.

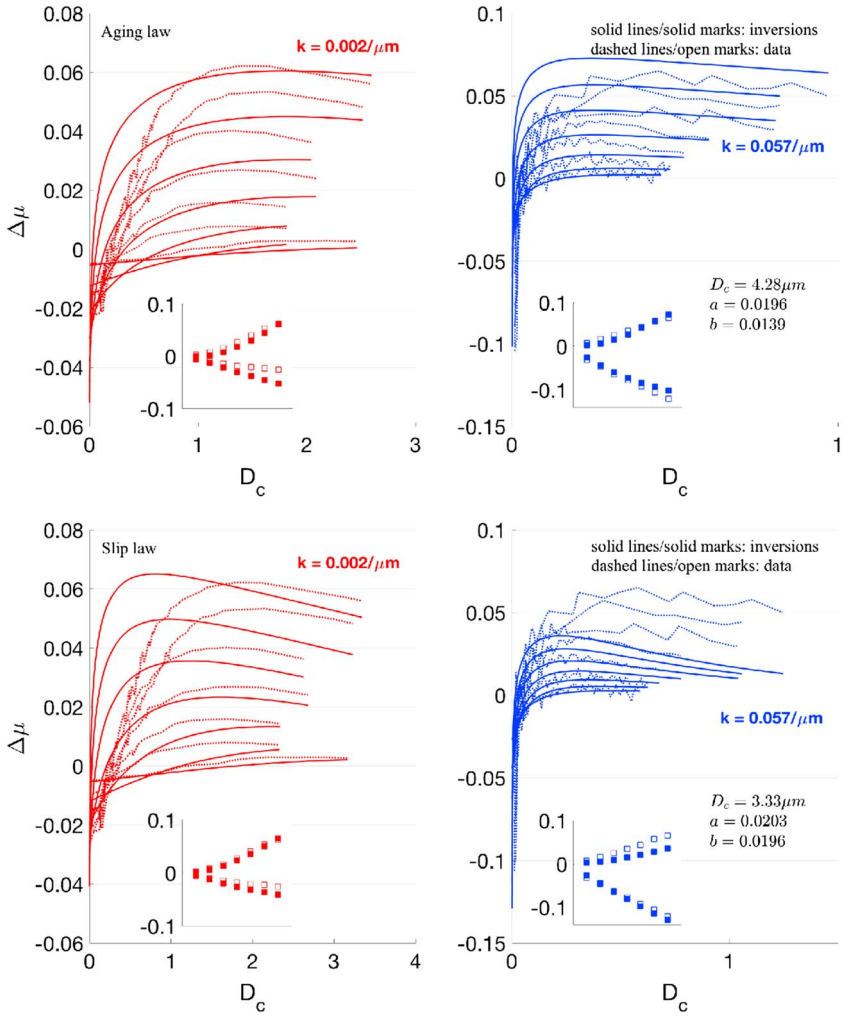

Figure 7. Finite series inversion results of Beeler et al. (1994) slide-hold-slide data using the Aging and the Slip law. Peaks and minima of the fitted finite series are shown in sets. Solid lines and open marks are simulations; dashed lines and solid marks are data. The Aging law matches the finite series well; the Slip law's fit is clearly inferior to the fit of our model (Figure 6). However, the best fit parameters of both the Aging law and the Slip law are not consistent with the physical condition of the experimental sliding surfaces (a-b has the wrong sign).

3.4. Bounds on S_c (The Characteristic Slip Length of Slip Strengthening)

While there is a well-constrained range for r_c ($r_c \in [0, 1]$), mathematically there is no upper bound for s_c. This parameter could be seen as controlling the completeness of the evolution of the asperity intrinsic strength: a small s_c corresponds to the situation where a large portion of different asperity size classes could evolve to a relatively complete level; on the contrary, under a large s_c, even after a long slip distance most asperities are still not much strengthened. Therefore, if $S_c \gg D_c$, then the slip-strengthening process becomes trivial and S_c is essentially not a functioning parameter. In addition, $S_c \gg D_c$ implies that the characteristic strain over which the strain-hardening occurs is $\gg 1$, which seems unlikely. For these reasons, we set an upper bound for s_c in the inversions ($s_c \leq 2$, suggested by tests). The best fit s_c in all our results falls away from this upper bound and lies near 1 (i.e., $S_c \approx D_c$), a good reference value under which it is a well-functioning parameter.

4. Discussion and Conclusion

This paper is among the first attempts in rate and state friction studies to model friction evolution assuming both time dependence and slip dependence. We propose a new model which relies on the ideas from a number of previous studies, including the observed time-dependent area growth (Dieterich & Kilgore, 1994), the unequivocal slip dependence suggested by well-fit velocity steps (Bhattacharya et al., 2015), and the

two-scale structural description of friction evolution (Li & Rubin, 2017). In order to reconcile the two aspects of RSF, the model combines the time-dependent contact area growth with a slip-strengthening process, which could be associated with the strain-hardening mechanism (Mott, 1952). This combined mechanism has an improved physical picture than the purely empirical Aging and Slip laws, since both the contact area growth and the slip-strengthening effect could be supported by the plastic behaviors of asperities on the frictional surface. In our new model, the two macroscopic coefficients (a, b) in classical RSF equations are grounded by microscopic definitions, and two new parameters (r_c and s_c) are introduced to specify the slip-strengthening curve. Moreover, by amplifying the parameter space, this model incorporates a pure aging law, which is highly similar to the classical Aging law, as a subset. We demonstrated the model behavior through simulations and then used the model to invert the experimental friction data.

Results show that the quality of this model's best fit to the SHS data is similar to the best fit of the Slip law, but the results of our model are closer to the frictional properties of the experimental sliding surface. However, unfortunately, we found that our model was not able to recover the symmetry of the velocity steps to the extent displayed by the Slip law, although it produced acceptable fits to low-order finite stiffness velocity steps. This might result from the fact that in the current model we assume a simplified form of the slip-strengthening mechanism that the evolution of the asperities' intrinsic strength only depends on the in-contact slip δ. It is known that strain hardening may also depend on strain rate and temperature, in a nonlinear fashion (Mecking & Kocks, 1981). In the parameter setting of the current model, a possible future trial could be further assuming that the slip strengthening depends on the sliding velocity, that is, $\hat{\tau} = \hat{\tau}(\delta, V)$ with V appears in the exponential (equation (10)), although this will inevitably introduce extra parameters. Generally speaking, it is expected that a more detailed mathematical description of the frictional surface, together with the introduction of high-order physical mechanisms, would help improve the resolution of the current model and thus improve its fitting performance.

Upon the original model, we investigated a variant of the model assuming an extra physical mechanism regarding the asperity contact that only the commensurate areas of the contacting asperity portions, instead of two different areas from both sides of the contact, contribute to the total asperity strength. In other words, when a larger older asperity portion confronts with a smaller newer portion, the strength from some part of the older portion is not counted due to incommensuration of the two areas. Therefore, instead of averaging contact areas from both sides, we select the smaller area from the two sides and regard it as the true contact area. We compare this variant of the model with the original model without the commensurate assumption. Results show that adding this new assumption helps increase the symmetry for velocity step curves (Figure 3c). Nevertheless, it is difficult to argue that adopting this assumption could certainly add to the physical base of the model, since it considers the commensuration of individual portions rather than over the entire asperity, the latter being more realistic. This extra mechanism is also extremely costly in computation, and therefore, this model variant is infeasible to be used in inversions.

Given the fact that our model has introduced two new parameters compared with the classical RSF equations, yet has not much improved the fits to the experimental data of either velocity steps or SHS, one may argue if this model is better than a traditional RSF model with multiple state variables (Ruina, 1983). Unfortunately, we do not have a clear answer for this question. It is true that in many cases adding more parameters will often help improve the fitting performance, and we nevertheless did the other way around by failing to make much improvement; adding one or two more state variables to the traditional RSF model will potentially yield better fitting results. However, state variables not well grounded by physics are invalid and the fitting performance could always be enhanced by adding arbitrary parameters; it is exactly for this reason that people decided to adopt only one state variable in the RSF theory in case that the physics are compromised. It is clear that the introduction of the two new parameters in our model is not arbitrary and is supported by well-defined physical assumptions. Therefore, in this sense, it is not obvious that our model is inferior to a potential RSF model with multiple state variables, although it is also not valid to claim that this model is better, given that the fitting results are not decisively convincing.

This model is deficient in a number of aspects. A major drawback is that its geometrical configuration of the area growth is unsettled. In the model, asperity portions are heterogeneous in the slip direction and homogeneous in the slip-perpendicular direction and we thus have to assume that contact area only grows perpendicularly. One would also argue that more realistically the new area of an asperity will appear from its edge rather than from its interior portions, as is assumed in this model (growth on all of the grid

elements). A possible yet untestable fix for this problem could be adding an extra assumption that asperity portions are actually unfilled but instead has a smaller core or consists smaller atomic bonds, in which case there is some space for it to grow. However, since our discretization scale $\Delta\delta$ is not fixed and determined by numerical considerations, this alternative picture of asperities is also flawed because grid elements should not be allowed to be unfilled at all scales. Moreover, we assume implicitly in the model that the new area is completely lost when the asperity leaves contact, which is free of contact thereafter for a certain period of time, and therefore, asperity portions periodically reclaim the original contact area. This implies some elastic behavior of the asperities, which might be contradictory to our assumption of the plastic behavior (slip strengthening) of asperities. Further elaboration of the physical mechanisms on frictional surfaces is expected to resolve this problem. Lastly, our model is developed from the asperity interactions on the bare rock surface, and we use it to fit the data obtained from synthetic gouges as well. Ideally, the RSF law should apply to various frictional settings; however, the applicability of a microscopic structural model to different physical settings should not be taken for granted. Indeed, it is likely that for the exact reason the model's fit to the current velocity steps data set from gouges is not as *satisfying*, but this claim is unwarranted and the applicability of the model is expected to be further tested in future work.

Two methodological insights emerge from this study, which are probably marginal to traditional geophysical studies. First, it is worth mentioning that the two-scale numerical framework used in our model embodies the concept of agent-based modeling, a term more commonly appearing in social science (e.g., Bonabeau, 2002). To obtain the state variable Θ, we abandoned the usage of ODEs and instead numerically simulated the frictional surface by keeping track of the behavior of different asperities (agents). Since asperities of different sizes behave differently due to their different "memory potential" in recording past velocity histories, this agent-based approach is expected to be of higher resolution than ODEs (e.g., the Aging law or Slip law) which generalize the behaviors of all agents. Second, it is also interesting to note that the memory-recording kernel (F) in our model essentially embodies the idea used in recurrent neural networks. In both cases, a consecutive input series (in our model, V) consistently modifies a memory kernel and drives the output series (in our model, Θ; e.g., LeCun et al., 2015). We would like to pin down these two points, but it is audacious to claim that these philosophies would have further implications for future investigations of the RSF theory. However, since the two existing laws (the Aging law and the Slip law) were raised at a time when large-scale computation was not always possible, and now we are having more powerful numerical tools, it will always be a promising direction to try to readdress this old problem of friction through more advanced approaches, and this study may serve as a first attempt. We demonstrated the great potential of a granular construction of the interactive physical picture for high-resolution frictional studies, in replacement of the traditional laws in the form of ODEs. Such a structural model is convenient for the implementation and testing of elaborated physical mechanisms on the frictional interface, and the results of the current model, not as satisfactory as expected, might be improved through such elaborations in future work. Given that these attempts will inevitably enlarge the model's parameter space, correspondingly, it is also expected that a number of new laboratory experiments are to be designed in order to provide better empirical constraints for models of this kind.

Acknowledgments
The author wishes to thank Prof. Allan Rubin at Princeton Geosciences for his countless valuable instructions throughout and beyond the author's study of friction, in particular, whose suggestions on the current project greatly helped improve the quality of this research. The author thanks Chris Marone, Brett Carpenter, Martijn van den Ende, Jean-Paul Ampuero, and an anonymous reviewer for valuable comments that helped refine the earlier drafts of this paper. The velocity step data (P1060) are available from Bhattacharya et al. (2015) and the Rock and Sediment Mechanics Laboratory, Penn State University; the SHS data are available from Beeler et al. (1994) and Brown University. This research was funded by the National Science Foundation (NSF) under award EAR-1547286.

References

Aharonov, E., & Scholz, C. H. (2018). A physics-based rock friction constitutive law: Steady state friction. *Journal of Geophysical Research: Solid Earth*, *123*, 1591–1614. https://doi.org/10.1002/2016JB013829

Ampuero, J.-P., & Rubin, A. M. (2008). Earthquake nucleation on rate and state faults—Aging and slip laws. *Journal of Geophysical Research*, *113*, B01302. https://doi.org/10.1029/2007JB005082

Baumberger, T., & Caroli, C. (2006). Solid friction from stick-slip down to pinning and aging. *Advances in Physics*, *55*(3-4), 279–348.

Bayart, E., Rubin, A. M., & Marone, C. (2006). *Evolution of fault friction following large velocity jumps*. AGU Fall Meeting Abstracts.

Beeler, N., Tullis, T., & Weeks, J. (1994). The roles of time and displacement in the evolution effect in rock friction. *Geophysical Research Letters*, *21*(18), 1987–1990.

Bhattacharya, P., Rubin, A. M., Bayart, E., Savage, H. M., & Marone, C. (2015). Critical evaluation of state evolution laws in rate and state friction: Fitting large velocity steps in simulated fault gouge with time-, slip-, and stress-dependent constitutive laws. *Journal of Geophysical Research: Solid Earth*, *120*, 6365–6385. https://doi.org/10.1002/2015JB012437

Bhattacharya, P., Rubin, A. M., & Beeler, N. M. (2017). Does fault strengthening in laboratory rock friction experiments really depend primarily upon time and not slip? *Journal of Geophysical Research: Solid Earth*, *122*, 6389–6430. https://doi.org/10.1002/2017JB013936

Bhattacharya, P., Rubin, A. M., Tullis, T., Okazaki, K., & Beeler, N. M. (2016). Where did the time go? Friction evolves with slip following large velocity steps, normal stress steps and during long holds. AGU Fall Meeting.

Bonabeau, E. (2002). Agent-based modeling: Methods and techniques for simulating human systems. *Proceedings of the National Academy of Sciences*, *99*(suppl 3), 7280–7287.

Dieterich, J. H. (1979). Modeling of rock friction: 1. Experimental results and constitutive equations. *Journal of Geophysical Research*, *84*(B5), 2161–2168.
Dieterich, J. H., & Kilgore, B. D. (1994). Direct observation of frictional contacts: New insights for state-dependent properties. *Pure and Applied Geophysics*, *143*(1-3), 283–302.
Dieterich, J. H., & Kilgore, B. (1996). Implications of fault constitutive properties for earthquake prediction. *Proceedings of the National Academy of Sciences*, *93*(9), 3787–3794.
Du, N., Yang, Z., Liu, X. Y., Li, Y., & Xu, H. Y. (2011). Structural origin of the strain-hardening of spider silk. *Advanced Functional Materials*, *21*(4), 772–778.
Greenwood, J. A., & Williamson, J. B. P. P. (1966). Contact of nominally flat surfaces, *Proceedings of The Royal Society A Mathematical Physical and Engineering Sciences*, *295*(1442), 300–319.
Hatano, T. (2015). Friction laws from dimensional-analysis point of view. *Geophysical Journal International*, *202*(3), 2159–2162.
Ikari, M. J., Carpenter, B. M., & Marone, C. (2016). A microphysical interpretation of rate-and state-dependent friction for fault gouge. *Geochemistry, Geophysics, Geosystems*, *17*, 1660–1677. https://doi.org/10.1002/2016GC006286
Karner, S. L., & Marone, C. (2001). Fractional restrengthening in simulated fault gouge: Effect of shear load perturbations. *Journal of Geophysical Research*, *106*(B9), 19,319–19,337.
Kato, N., & Tullis, T. E. (2001). A composite rate-and state-dependent law for rock friction. *Geophysical Research Letters*, *28*(6), 1103–1106.
LeCun, Y., Bengio, Y., & Hinton, G. (2015). Deep learning. *Nature*, *521*(7553), 436–444.
Li, T., & Rubin, A. M. (2017). A microscopic model of rate and state friction evolution. *Journal of Geophysical Research: Solid Earth*, *122*, 6431–6453. https://doi.org/10.1002/2017JB013970
Li, J., Weng, G. J., Chen, S., & Wu, X. (2017). On strain hardening mechanism in gradient nanostructures. *International Journal of Plasticity*, *88*, 89–107.
Marone, C. (1998). The effect of loading rate on static friction and the rate of fault healing during the earthquake cycle. *Nature*, *391*(6662), 69–72.
Marone, C., & Saffer, D. M. (2015). The mechanics of frictional healing and slip instability during the seismic cycle, *Earthquake Seismology* (pp. 111–138). B.V: Elsevier Inc.
Mecking, H., & Kocks, U. F. (1981). Kinetics of flow and strain-hardening. *Acta Metallurgica*, *29*(11), 1865–1875.
Mott, N. F. (1952). CXVII. A theory of work-hardening of metal crystals. *The London, Edinburgh, and Dublin Philosophical Magazine and Journal of Science*, *43*(346), 1151–1178.
Nagata, K., Kilgore, B., Beeler, N., & Nakatani, M. (2014). High-frequency imaging of elastic contrast and contact area with implications for naturally observed changes in fault properties. *Journal of Geophysical Research: Solid Earth*, *119*, 5855–5875. https://doi.org/10.1002/2014JB011014
Nagata, K., Nakatani, M., & Yoshida, S. (2012). A revised rate- and state-dependent friction law obtained by constraining constitutive and evolution laws separately with laboratory data. *Journal of Geophysical Research*, *117*, B02314. https://doi.org/10.1029/2011JB008818
Nakatani, M. (2001). Conceptual and physical clarification of rate and state friction: Frictional sliding as a thermally activated rheology. *Journal of Geophysical Research*, *106*(B7), 13,347–13,380.
Nakatani, M., & Scholz, C. H. (2006). Intrinsic and apparent short-time limits for fault healing: Theory, observations, and implications for velocity-dependent friction. *Journal of Geophysical Research*, *111*, B12208. https://doi.org/10.1029/2005JB004096
Nes, E. (1997). Modelling of work hardening and stress saturation in FCC metals. *Progress in Materials Science*, *41*(3), 129–193.
Niemeijer, A., Marone, C., & Elsworth, D. (2008). Healing of simulated fault gouges aided by pressure solution: Results from rock analogue experiments. *Journal of Geophysical Research*, *113*, B04204. https://doi.org/10.1029/2007JB005376
Niemeijer, A., Marone, C., & Elsworth, D. (2010). Frictional strength and strain weakening in simulated fault gouge: Competition between geometrical weakening and chemical strengthening. *Journal of Geophysical Research*, *115*, B10207. https://doi.org/10.1029/2009JB000838
Press, W. H., Teukolsky, S. A., Vetterling, W. T., & Flannery, B. P. (1986). Downhill simplex method in multidimensions. *Numerical Recipes: The Art of Scientific Computing*, *10*, 289–293.
Rabinowicz, E. (1951). The nature of the static and kinetic coefficients of friction. *Journal of Applied Physics*, *22*(11), 1373–1379.
Rabinowicz, E. (1958). The intrinsic variables affecting the stick-slip process. *Proceedings of the Physical Society*, *71*(4), 668.
Rathbun, A. P., & Marone, C. (2013). Symmetry and the critical slip distance in rate and state friction laws. *Journal of Geophysical Research: Solid Earth*, *118*, 3728–3741. https://doi.org/10.1002/jgrb.50224
Renard, F., Beauprêtre, S., Voisin, C., Zigone, D., Candela, T., Dysthe, D. K., & Gratier, J. P. (2012). Strength evolution of a reactive frictional interface is controlled by the dynamics of contacts and chemical effects. *Earth and Planetary Science Letters*, *341*, 20–34.
Rice, J. R., Lapusta, N., & Ranjith, K. (2001). Rate and state dependent friction and the stability of sliding between elastically deformable solid. *Journal of the Mechanics and Physics of Solids*, *49*(9), 1865–1898.
Rubin, A. M., & Ampuero, J. P. (2005). Earthquake nucleation on (aging) rate and state faults. *Journal of Geophysical Research*, *110*, B11312. https://doi.org/10.1029/2005JB003686
Ruina, A. (1983). Slip instability and state variable friction laws. *Journal of Geophysical Research*, *88*(12), 10,359–10,370.
Sleep, N. H. (2005). Physical basis of evolution laws for rate and state friction. *Geochemistry, Geophysics, Geosystems*, *6*, Q11008. https://doi.org/10.1029/2005GC000991
Tullis, T. E., & Weeks, J. D. (1986). Constitutive behavior and stability of frictional sliding of granite. *Pure and Applied Geophysics*, *124*(3), 383–414.
Van Melick, H. G. H., Govaert, L. E., & Meijer, H. E. H. (2003). On the origin of strain hardening in glassy polymers. *Polymer*, *44*(8), 2493–2502.
van den Ende, M., & Niemeijer, A. (2018). Time-dependent compaction as a mechanism for regular stick-slips. *Geophysical Research Letters*, *45*, 5959–5967. https://doi.org/10.1029/2018GL078103